(3) Leary, D. F.; Williams, M. C. *J. Polym. Sci., Part B* **1970**, *B8*, 335.
(4) LeGrand, D. G. *Polym. Prepr., Am. Chem. Soc., Div. Polym. Chem.* **1970**, *11*, 434.
(5) Meier, D. J. *Appl. Polym. Symp.* **1974**, 24, 67 and prior work cited therein.
(6) Bajaj, P.; Varshney, S. K. *Polymer* **1980**, *21*, 201.
(7) Kambour, R. P. "Block Copolymers"; Aggarwal, S. L., Ed.; Plenum Press: New York-London, 1970; p 263.
(8) Wilkes, G. L.; Emerson, J. A. *J. Appl. Phys.* **1976**, *47*, 4261.
(9) Aggarwal, S. L. *Polymer* **1976**, *17*, 938.
(10) Kambour, R. P. *J. Polym. Sci., Part B* **1969**, *B7*, 573.
(11) LeGrand, D. G. *J. Polym. Sci., Part B* **1969**, *B7*, 579.
(12) Hashimoto, T.; Fujimura, M.; Kawai, H. *Macromolecules* **1980**, *13*, 1660.
(13) Richards, R. W.; Thomason, J. L. *Polymer* **1981**, *22*, 581.
(14) Russell, T. P.; Stein, R. S. *J. Polym. Sci.* **1982**, *20*, 1593.
(15) Morêse-Séguéla, B.; St.-Jacques, M.; Renard, J. M.; Prud'homme, J. *Macromolecules* **1980**, *13*, 100.
(16) Gaur, U.; Wunderlich, B. *Macromolecules* **1980**, *13*, 1618.
(17) Krause, S.; Iskandar, M. *Adv. Chem. Ser.* **1979**, *No 176*, 205.
(18) Brown, I. M. *Macromolecules* **1981**, *14*, 801.
(19) LeGrand, D. G. *J. Rheol. (N. Y.)* **1971**, *15*, 541.
(20) Assink, R. A. *Macromolecules* **1978**, *11*, 1233.
(21) Lind, A. C. *J. Chem. Phys.* **1977**, *66*, 3482.
(22) Wardell, G. E.; McBrierty, V. J.; Douglass, D. C. *J. Appl. Phys.* **1974**, *45*, 3441.
(23) Vaughn, H. A., Jr. *J. Polym. Sci., Part B* **1969**, *B7*, 569.
(24) Fox, T. G.; Flory, P. J. *J. Appl. Phys.* **1950**, *21*, 581.
(25) Lind, A. C. *Bull. Am. Phys. Soc.* **1980**, *25*, 315.
(26) Bares, J. *Macromolecules* **1975**, *8*, 244.
(27) Couchman, P. R.; Karasz, F. E. *J. Polym. Sci., Polym. Symp. Ed.* **1978**, *63*, 271.
(28) Niznik, G. E.; LeGrand, D. G. *J. Polym. Sci., Polym. Symp. Ed.* **1977**, *60*, 97.
(29) Lind, A. C. *Rev. Sci. Instrum.* **1972**, *43*, 1800.
(30) Pebbles, L. H., Jr. *Macromolecules* **1976**, *9*, 58.
(31) For the BPAC/DMS synthesis conditions employed here, the $n = 1$ BPA blocks were formed during end capping, while the $n \geq 2$ BPAC blocks were independently formed during the second stage of polymerization. A modified binomial distribution function incorporating these features was employed, but the errors in the NMR data did not justify its use.
(32) Desa, J. A. E.; Brown, I. M.; Lind, A. C.; Sandreczki, T. C. *Am. Crystallogr. Assoc., Ser. 2* **1983**, *11*, 36.
(33) Mercier, J. P.; Aklonis, J. J.; Litt, M.; Tobolsky, A. V. *J. Appl. Polym. Sci.*, **1965**, *9*, 447.
(34) Merrill, S. H.; Petrie, S. E. *J. Polym. Sci., Part A* **1965**, *3*, 2189.
(35) Williams, A. D.; Flory, P. J. *J. Polym. Sci., Part A-2* **1968**, *6*, 1945.

Phase Diagrams and Morphology of a Urethane Model Hard Segment and Polyether Macroglycols

Kirk K. S. Hwang,† David J. Hemker, and Stuart L. Cooper*

Department of Chemical Engineering, University of Wisconsin, Madison, Wisconsin 53706.
Received May 19, 1983

ABSTRACT: Binary mixtures of a urethane hard-segment model compound, diethyl 4,4′-methylenebis(*N*-phenylcarbamate) (H_1), and various polyether macroglycols have been investigated by means of differential scanning calorimetry, wide-angle X-ray diffractometry, and optical microscopy. Both poly(ethylene oxide) (1500 MW) and poly(tetramethylene oxide) (1000 MW) form a eutectic with H_1 in weight ratios of H_1/PEO (40/60) and H_1/PTMO (20/80). Poly(propylene oxide) and H_1 mix to form a crystalline–amorphous blend. X-ray diffraction patterns showed that the presence of polyether macroglycols caused no change in the crystal structure of H_1 crystals in the blends. This suggests that the melting point depression observed is explicable in terms of H_1–polyol thermodynamic mixing. On the basis of Scott's equation, the interaction parameter densities of H_1/PEO, H_1/PTMO, and H_1/PPO were determined to be −4.63 cal/cm^3, −3.42 cal/cm^3, and −1.21 cal/cm^3, respectively, at the H_1 melting point. Optical microscopy revealed that H_1 spherulites were larger in size and more perfect in texture in the blends of H_1 and polyols than in pure H_1.

Introduction

The morphology and physical properties of diphenylmethane diisocyanate (MDI) based segmented polyurethanes have been studied extensively[1-4] and have been found to depend on several factors such as the composition ratio of urethane and polyether segments, the molecular weight of the individual segments, and segmental compatibility.

In this study, the segmental compatibility of urethane hard segments and polyether soft segments was investigated by determining the phase diagrams of physical mixtures of a model hard segment with various macroglycols. Diethyl 4,4′-methylenebis(*N*-phenylcarbamate) (designated as H_1), which is the repeating unit of the MDI–butanediol (BD) hard segment, served as the hard-segment model compound. Poly(ethylene oxide) (PEO), poly(propylene oxide) (PPO), and poly(tetramethylene oxide) (PTMO) macroglycols were used to model the soft segment.

A recent study by Camberlin[5] showed that the hard-segment model compound diethyl 4,4′-methylenebis(*N*-phenylcarbamate) displays a melting point of 125 °C in its initial stable form and 99.7 °C in its metastable form. Blackwell[6] studied a similar model compound of the urethane hard segment, dimethyl 4,4′-methylenebis(*N*-phenylcarbamate), using X-ray diffraction. This model compound was found to possess a monoclinic structure with four molecules in each unit cell. However, he also reported an oriented MDI/BD hard segment in a triclinic structure.[7,8]

The crystalline structures of poly(ethylene oxide) (PEO) and poly(tetramethylene oxide) (PTMO) have been studied extensively by a number of authors using X-ray scattering and IR spectroscopy.[9-12] PEO was found to possess a monoclinic helical structure with four repeating units in each unit cell, and PTMO was found to possess a planar zigzag monoclinic structure with two repeating units in each unit cell. Atactic poly(propylene oxide) is an amorphous material.

When two crystalline polymers or one crystalline and one amorphous polymer are mixed together, the miscibility of the two components with respect to composition and

† Present address: Life Sciences Sector Lab, 3M Co., St. Paul, MN 55144.

0024-9297/84/2217-0307$01.50/0

temperature can be represented in a phase diagram. In the analysis of polymer–polymer phase diagrams, Scott's treatment of polymer mixtures based on the classical Flory–Huggins equation is widely used to calculate the spinodal and binodal compositions and the melting point depression.[13-16] In this theory, the chemical potential (μ_{2u}) or activity (a_{2u}) of a structure unit of component 2 in a binary polymer solution can be expressed as

$$(\mu_{2u} - \mu^\circ_{2u})/RT = \frac{V_{2u}}{V_{1u}M_2}\left[\ln \phi_2 + \left(1 - \frac{M_2}{M_1}\right)\phi_1 + \chi M_2 \phi_1^2\right] = \ln a_2 \quad (1)$$

where subscript 1 represents the polymer which is considered as a diluent for polymer 2, and V_{2u} is the molar volume of the structural unit of polymer component 2. ϕ_2 is the volume fraction and M_2 is the degree of polymerization of polymer 2, and χ is the interaction parameter. The activity coefficient of the structural unit of component 2 in the mixture is expressed as

$$\ln \gamma_2 = \frac{V_{2u}}{V_{1u}M_2}\left[\left(1 - \frac{M_2}{M_1}\right)\phi_1 + \chi M_2 \phi_1^2\right] \quad (2)$$

The molar excess Gibbs free energy due to mixing can then be written as

$$G^E = RT(\phi_1 \ln \gamma_1 + \phi_2 \ln \gamma_2) \quad (3)$$

where

$$G^E = H^E - TS^E \quad (4)$$

When G^E has a negative value, mixing is thermodynamically favored.

In this work, phase diagrams of three binary mixtures of a urethane hard-segment model compound, H_1, and polyether soft-segment model compounds, PEO, PPO, and PTMO, were analyzed. The interaction parameter density, B, in the blends was determined from the depression of the hard-segment melting point. Wide-angle X-ray diffraction was used to analyze the diffraction characteristics of the H_1–polyol blends at various compositions and temperatures. In addition, the effect of composition on the spherulite size of the crystalline blends at a given temperature was studied using a polarizing optical microscope.

Experimental Section

Materials. The materials studied include diethyl 4,4′-methylenebis(*N*-phenylcarbamate) (coded H_1) and its blends with three polyethers of different oxygen to carbon ratios. These are poly(ethylene oxide) (PEO) of 1500 MW obtained from Aldrich, poly(propylene oxide) (PPO) of 1000 MW obtained from BASF Wyandotte, and poly(tetramethylene oxide) (PTMO) of 1000 MW obtained from Quaker Oats. The hard-segment model compound (H_1) was made by capping MDI with ethanol. The synthesis was carried out by stirring 4,4′-methylenebis(phenyl isocyanate) with excess ethanol at 50 °C. As the reaction proceeded, H_1 precipitated as a white product. After an IR trace showed that no isocyanate residue remained in the ethanol solution, the model compound was collected by vacuum filtration. H_1 was dried in a vacuum oven at 50 °C for 1 week and its purity assessed by NMR and gel permeation chromatography.

Blends of H_1/PEO, H_1/PPO, and H_1/PTMO were prepared from dilute THF solutions (1% by weight). The THF was slowly evaporated at room temperature to allow the components to mix at close to equilibrium conditions. A week was normally allowed for precipitation and mild drying of the blends. The blends were further dried under vacuum for 2 weeks at 25 °C.

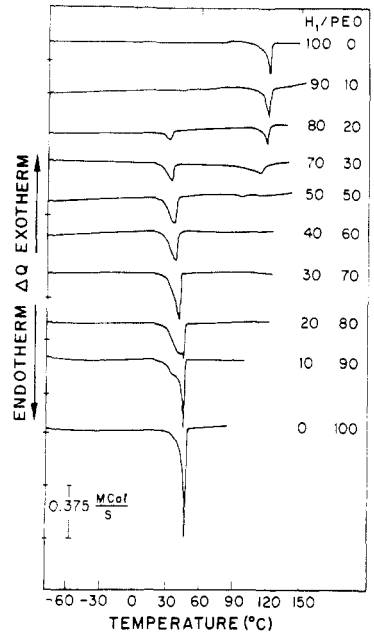

Figure 1. DSC thermograms of H_1/PEO blends.

Characterization. Density Measurement. The densities of the hard-segment model compound (H_1) and soft-segment polyols in their molten states were measured by a pycnometer using ASTM method D-70. The volume of the pycnometer was calibrated with mercury at various temperatures.

Differential Scanning Calorimetry (DSC). DSC measurements were conducted on a Perkin-Elmer DSC-2 which was calibrated with mercury and indium standards to ±0.2 °C. The melting point of the pure materials and their blends were defined by the onset of the melting endotherms.[17] The liquidus point of the blends is reported as the minimum in the endothermic melting peak. A heating rate of 5 °C/min under a He atmosphere was used in all cases.

Wide-Angle X-ray Diffraction. Wide-angle X-ray diffraction (WAXD) experiments were performed on ~0.5-mm thick solvent cast samples with a Picker Model 3667A diffractometer. A sealed X-ray tube generator with a Cu Kα target (λ 1.542 Å) which operated at 35 kV and 15 mA provided the source of X-rays. Data were obtained from 3° to 40° with a time constant of 1 s. The slit system used had a Gaussian weighting function with a 1° full width at half-maximum. Intensity was plotted as counting rate vs. angle on a strip chart recorder.

Optical Microscopy. Spherulites were photographed with a Polaroid camera attached to a Carl Zeiss polarizing microscope. Samples were cast on the surface of glass plates and dried in a vacuum oven in a similar fashion to those prepared for thermal analysis.

Results and Discussion

Thermal Analysis. Differential scanning calorimetry was used to determine the phase diagrams of blends of the polyols with the hard-segment model compounds. In each system, the composition ratio of H_1/polyol was varied from 100/0 to 0/100. DSC traces of the three systems studied are shown in Figures 1–3. The thermograms of each blend were recorded from −100 to 135 °C at a heating rate of 5 °C/min. Various heating rates (20, 10, 5, 2.5, and 1.25 °C/min) were first used on selected blends of H_1 with the polyols. At 5 °C/min the effect of heating rate on the thermal transitions in the blends begins to level off. This heating rate, which allows reasonable sensitivity and rate of testing, allows the molecules in the blend to redistribute close to their equilibrium compositions with respect to the variation in temperature.

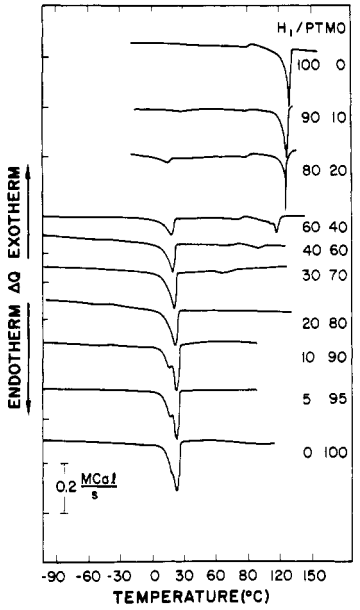

Figure 2. DSC thermograms of H_1/PTMO blends.

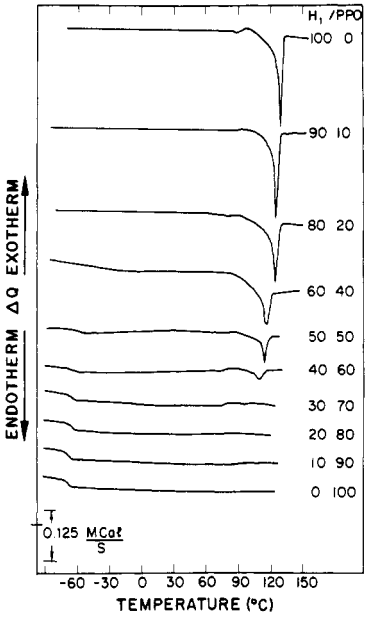

Figure 3. DSC thermograms of H_1/PPO blends.

Figure 1 shows the thermograms of the H_1/PEO system. The melting point of pure H_1 appears at 128.5 °C, which is in close agreement with the 128 °C obtained by Nakayama.[18] Recently, a T_m of 125 °C has been reported by Camberlin.[5] In the thermogram of H_1 a small endotherm was observed at 87 °C, immediately followed by an exotherm at 97 °C. This is believed to be due to the melting and recrystallization of H_1 semicrystalline regions in which defects are present. These lower temperature thermal events can be eliminated by annealing at 77 °C for 10 min. As PEO was blended into H_1, the temperature range of the small endotherms and exotherms due to H_1 as well as its sharp melting point decreased. When the amount of PEO added was greater than 20% (wt %), a lower melting temperature was observed at 31 °C. The onset of this second T_m appeared at the same temperature regardless of the variation in composition, and its area became larger as the concentration of PEO increased. It was also observed that the melting point of the hard segments and the peak area associated with it decreased as the hard-segment content decreased. This melting point completely

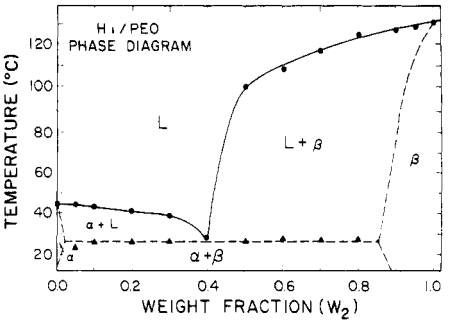

Figure 4. Phase diagram of the H_1/PEO blend system. Liquidus points are shown by circles, and eutectic points by triangles. The solidus lines at both ends of the phase diagram are estimated.

disappeared at the composition of 40/60 (H_1/PEO). With a further increase in the amount of PEO beyond 40/60 (H_1/PEO), a new melting point appeared immediately following the 31 °C melting point. In the range of 30/70 to 10/90 (H_1/PEO), these two melting peaks overlap to some extent. The area of the higher temperature melting peak increased with increasing amount of PEO. Finally, pure PEO displayed a melting point with an onset at 45 °C and peak maximum at 47 °C.

It is typical that binary mixtures giving rise to eutectic phase diagrams exhibit two melting peaks.[19] The rather sharp lower temperature endotherm, which appears at about 31 °C, is assigned to the melting of the eutectic fraction, whereas the high temperature endotherm is attributed to the melting of either the H_1 or PEO solid solution. On the basis of thermal transitions of the H_1/PEO system obtained from Figure 1, a typical eutectic phase diagram with a eutectic composition at 40/60 (H_1/PEO) can be constructed as shown in Figure 4. The melting point of the eutectic mixture was about 31 °C. Since no eutectic melting was observed for samples with compositions of 95/5 and 90/10 (H_1/PEO), a limited solid solution (designated as β) is suggested in this region of the diagram. The tie line calculations based on the ΔH at the eutectic melting of the blends show that the solid solution behavior may well extend to a composition close to 85/15 (H_1/PEO). A small solid solution (H_1 in PEO) (assigned as α) is also suggested for samples of high PEO content. This was not observed experimentally, possibly because the H_1 content was too low to be detected. The liquidus line was determined by taking the minimum points of the melting endotherms plotted as shown in Figure 4. Above the liquidus line, PEO and H_1 were in a well-mixed liquid state. The solidus line (dashed line) in the region rich in H_1 was qualitatively determined on the basis of the melting point onset. The eutectic isotherm on the solidus line was determined by the onset of the melting of the eutectic fraction. Below the eutectic isotherm, H_1 and PEO should phase separate into two crystalline forms (α and β), though the segmental diffusion rate may be slow and the sample may slowly, if ever, reach an equilibrium state.

Figure 2 shows the thermograms of the H_1/PTMO blends. The poly(tetramethylene oxide) macroglycol is different from poly(ethylene oxide) macroglycol in its lower content of ether groups, its lower melting point, and crystalline structure. As observed, pure PTMO displayed a melting point with an onset at 13 °C and a peak maximum at 23 °C. This was identified as the metastable melting point of PTMO (100 MW). The equilibrium melting point of high molecular weight PTMO was previously reported as having a peak maximum at 57 °C.[17] Similar to the H_1/PEO system, the H_1/PTMO system possesses a eutectic phase diagram (Figure 5). The eutectic isotherm is at 10 °C, and the eutectic composition

Table I
Characterization of Polyether Macroglycols and Their Interaction Parameters with H_1

sample	density	MW_u [a]	V_{1u} [b]	B, cal/cm^3 [c]	χ_{12} [d]	χ_{12} [e]
PEO	0.986	44.05	44.68	−4.63	−0.27	−0.26
PTMO	0.976	72.11	73.88	−3.45	−0.33	−0.20
PPO	1.004	53.08	52.87	−1.21	−0.08	−0.07

[a] Molecular weight per polyether macroglycol repeat unit. [b] Molar volume per polyether macroglycol repeat unit. [c] Interaction density between H_1 and polyether macroglycol per cm^3 of polyether macroglycol. [d] Flory interaction parameter, BV_{1u}/RT at 120 °C. [e] χ_{12} normalized by the molar volume of poly(ethylene oxide) macroglycol repeat unit at 120 °C.

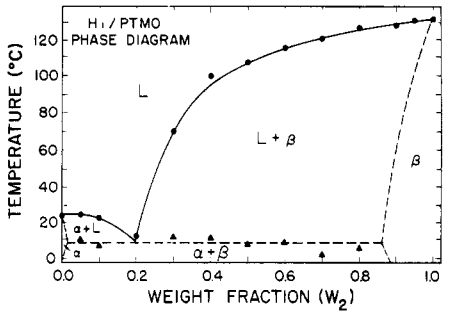

Figure 5. Phase diagram on the H_1/PTMO blend system. Liquidus points are shown by circles, and eutectic points by triangles. The solidus lines at both ends of the phase diagram are estimated.

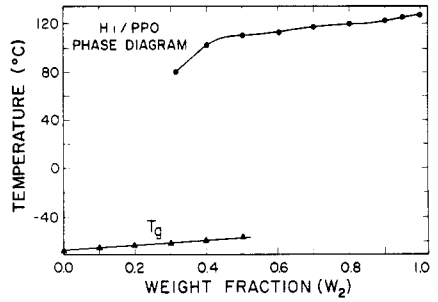

Figure 6. Phase diagram of H_1/PPO blends. Melting points are shown by circles and glass transition points are shown by triangles.

is found to contain 20% H_1. This is less concentrated in H_1 compared to the eutectic composition of the H_1/PEO system (40% H_1). Compositions of H_1/PTMO at 95/5 and 90/10 showing no eutectic melting suggest that there is a solid solution in the region which is rich in H_1.

Figure 3 shows the thermograms of the H_1/PPO system. The PPO added was amorphous, having a T_g at −71 °C. It was noticed that as H_1 was gradually diluted with PPO, the melting point of H_1 decreased at a slower rate compared to the H_1/PEO and H_1/PTMO systems (Figure 6). As the amount of PPO was increased to a composition of 50/50 (H_1/PPO), a distinct glass transition of PPO at −60 °C was observed in addition to the melting point of the hard segments. Further dilution with PPO caused the melting point of H_1 to disappear, the PPO glass transition temperature to appear at a lower temperature, and the ΔC_p in the transition zone to become larger. It was surprising that the presence of H_1 in PPO did not significantly affect the T_g of PPO, so that even with H_1/PPO in a ratio of 30/70 the T_g of PPO was only −64 °C (T_g of pure PPO = −71 °C). This suggests that the presence of H_1 causes little hindrance of rotation in the PPO backbone in the amorphous mixture when the concentration of H_1 is less than about 50%. However at H_1 concentrations above 50%, the PPO may exist as a finely divided phase inclusion whose T_g is not observable in the DSC experiment.

The melting point depression of H_1 caused by the addition of polyols in the mixture is similar to the melting point depression observed in many other crystalline polymer–diluent systems.[21,22] The equilibrium mixing of H_1 and polyols were analyzed by using the Scott equation.[13] The parameters used and results calculated are shown in Table I. For these systems the chemical potential, μ'_{2u}, per mole of H_1 unit in the mixture relative to its chemical potential μ°_{2u} in the pure liquid can be expressed as

$$\mu'_{2u} - \mu^\circ_{2u} = \frac{RTV_{2u}}{V_{1u}}\left[\frac{\ln \phi_2}{M_2} + \left(\frac{1}{M_2} - \frac{1}{M_1}\right)\phi_1 + \frac{BV_{1u}}{RT}\phi_1^2\right] \quad (5)$$

where the subscript 1 identifies the polyol and 2 H_1, ϕ is a volume fraction, V_u is the molar volume of the repeating units, M is the degree of polymerization, and B is the interaction energy density of the H_1–polyol mixture. If the entropy of mixing can be neglected, the Flory–Huggins interaction parameter, χ_{12}, is equivalent to BV_{1u}/RT.

The difference in the chemical potential between a crystalline H_1 unit (μ^c_{2u}) and the same unit in the pure liquid state (μ°_{2u}) can be written as

$$\mu^c_{2u} - \mu^\circ_{2u} = -(\Delta H_{2u} - T\Delta S_{2u}) \quad (6)$$

$$= -\Delta H_{2u}\left(1 - \frac{T}{T^\circ_m}\right) \quad (7)$$

where ΔH_{2u} and ΔS_{2u} are the enthalpy and entropy of fusion per mole of H_1 unit. The ratio $\Delta H_{2u}/\Delta S_{2u}$ is assumed to be independent of temperature and equal to T°_m, the equilibrium melting temperature. At the melting point of the mixture, the chemical potential of the H_1 unit in the crystalline and liquid phases are identical so one obtains from eq 5 and 7

$$\frac{1}{T_m} - \frac{1}{T^\circ_m} = -\frac{RV_{2u}}{\Delta H_{2u}V_{1u}}\left[\frac{\ln \phi_2}{M_2} + \left(\frac{1}{M_2} - \frac{1}{M_1}\right)\phi_1 + \frac{BV_{1u}}{RT}\phi_1^2\right] \quad (8)$$

To calculate B from eq 8, one must know the equilibrium melting point, T°_m, the heat of fusion of ΔH_{2u}, the density of H_1, and the density of the polyols. To determine T°_m of polymeric material experimentally, the Hoffman–Weeks method can be used. Unfortunately, since H_1 exists in a rather rigid phase, its diffusion rate may be too slow to maintain equilibrium during crystallization or ordering. This makes the Hoffman–Weeks method difficult to apply in order to obtain a vlaue of T°_m. In this study, a T°_m of H_1 (of 128.8 °C) was obtained by extrapolating the T_m of the H_1/polyol blends to zero polyol concentration. The ΔH°_{2u} of a hypothetically 100% crystalline sample of H_1 was determined to be 5.3 kcal/mol by applying Flory's equation (eq 9) to the melting temperatures of a series of monodisperse urethane oligomers[22]

$$\frac{1}{T_m} = \frac{1}{T^\circ_m} + \frac{R}{\Delta H_{2u}}\frac{2}{M} \quad (9)$$

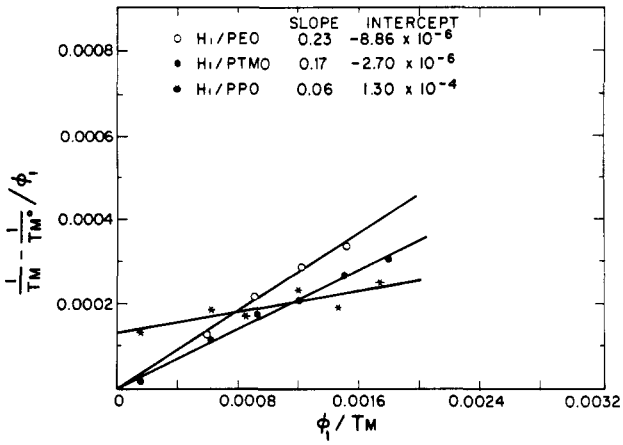

Figure 7. Plots of the quantity $(1/T_m - 1/T^\circ_m)/\phi_1$ against ϕ_1/T_m for H_1/PEO, H_1/PTMO, and H_1/PPO systems.

where M is the degree of polymerization. The densities of H_1, PTMO, PPO, and PEO, measured at each samples melting point, were 1.298, 0.977, 0.986, and 1.004 g/cm^3, respectively.

If the entropy terms can be neglected, eq 8 reduces to

$$\left(\frac{1}{T_m} - \frac{1}{T^\circ_m}\right) \Big/ \phi_1 = -\frac{V_{2u}B\phi_1}{\Delta H_{2u}T} \qquad (10)$$

In Figure 7, the data obtained in Figures 1–3 are plotted as $(1/\phi)[1/T_m - 1/T^\circ_m]$ vs. ϕ_1/T_m. For the H_1/PEO system, a least-squares fit of the data yields a straight line intersecting the vertical axis near zero. The slope of the straight line was 0.23 and the intercept was -8.8×10^{-6} K^{-1}. In view of the extremely small value of the ordinate intercept, the use of eq 10 appears justified. On the basis of values of V_{1u} of 44.68 cm^3/mol, V_{2u} of 263.69 cm^3/mol, and the slope, it was found that

$$B_{H_1/PEO} = -4.63 \text{ cal/cm}^3 \text{ (PEO)}$$

The Flory–Huggins interaction parameter, χ_{12}, between H_1 and the repeating unit of PEO is –0.26 ($\chi_{12} = BV_{1u}/RT$) at 120 °C.

In the system of H_1/PTMO, the plot suggested by eq 10 yields a straight line with a slope of 0.17 and an ordinate intercept of -2.7×10^{-6}. Again the small value of the ordinate intercept showed that the use of eq 10 was appropriate. The interaction density between H_1 and PTMO, $B_{H_1/PTMO}$, was found to be –3.42 cal/cm^3 (PTMO), and the χ_{12} between H_1 and the PTMO repeating unit, $-(CH_2)_4-O$, (V_{1u} = 73.88 cm^3/mol) was –0.32 at 120 °C. If the repeating unit of PTMO is chosen to have the same molar volume as the PEO repeating molar volume (44.68 cm^3/mol), χ_{12} would be –0.20 at 120 °C.

In the system of H_1/PPO, the data which test eq 10 fall on a straight line intersecting the ordinate at 1.29×10^{-4} with a slope of 6.08×10^{-2}. The interaction density $B_{H_1/PPO}$ was calculated to be –1.21. The χ_{12} between H_1 and the PPO repeating unit was –0.08 at 120 °C. If the repeating unit of PPO is normalized to have the same molar volume as the PEO repeating unit (44.68 cm^3/mol), the value of χ_{12} is –0.07 at 120 °C. Comparison of the data on all 3 systems reveals that the ordinate intercept in the H_1/PPO system was larger than that in the H_1/PTMO or H_1/PEO systems ($\sim 10^{-4}$ vs. $\sim 10^{-6}$). This may indicate that the entropy of mixing in the H_1/PPO system is more of a significant factor than in the other systems.

The negative value of χ_{12} or B for all three systems indicated that the three polyols can form a thermodynamically compatible mixture above the melting point of H_1. The most negative value of B appeared in the H_1/PEO system, suggesting that there was a strong interaction between H_1 and PEO. This could be due to PEO having a high concentration of ether oxygen which might interact with the urethane NH group in H_1. The PPO, which differs from PEO by having a methyl pendant group, showed the least interaction with H_1. This low interaction parameter could be due to a geometrical or conformational constraint caused by the methyl group on the PPO molecules which limits the intermolecular association.

Table II
Bragg Spacings for Crystalline H_1, PEO, and PTMO As Calculated from the WAXD Patterns

material	peak position, 2θ	Bragg spacing, Å	Bragg spacing[a] from ref 7, Å
H_1	9.1	9.71	
	11.5	7.68	7.65 (004)
	14.0	6.32	
	14.4	6.14	
	17.0	4.95	4.91 (102)
	18.2	4.87	
	18.5	4.79	4.75 (101)
	19.4	4.57	4.60 (014)
	19.7	4.50	4.53 (106)
	21.6	4.10	4.15 (107)
	22.5	3.95	
	23.0	3.86	3.89 (102)
	23.9	3.72	3.75 (018)
	24.2	3.67	
	25.3	3.52	3.56 (103)
			3.49 (119)
	26.7	3.35	
	27.0	3.30	3.30 (104)
	28.0	3.18	
	28.4	3.14	
PEO[b]	19.0	4.66	
	23.3	3.82	
PTMO[b]	20.2	4.40	
	24.7	3.60	

[a] Calculated for given reflection plane assuming a triclinic unit cell with a = 5.05 Å, b = 4.67 Å, c = 37.9 Å, α = 116°, β = 116°, and γ = 83.5° as proposed for crystalline MDI/BD by Blackwell, Nagarajan and Hoitink (ref 7). [b] Only the significant diffraction peaks of PEO and PTMO are reported.

Wide-Angle X-ray Diffraction. The interaction parameter densities in the blends were determined from the hard-segment melting point depressions by thermal analysis. This procedure is correct if the change in the free energy of the blend is solely due to mixing of the components and not to any crystalline transformation, change in the crystallite thickness, or a combination thereof. To confirm the validity of our analysis, the X-ray diffraction characteristics of the blends with respect to composition and temperature were studied.

The diffraction intensity was recorded from 3° to 40° (2θ). The locations of the diffraction maxima primarily serve to determine d spacings in the Bragg equation. The breadth of the diffraction peak is dependent on the size and perfection of the crystallites while the intensity is largely determined by the structure factors taking account of phase differences in the diffraction process. Figure 8 shows the wide-angle X-ray diffraction curves for pure H_1, PEO, and PTMO. A list of the diffraction peaks is given in Table II. Many of the Bragg spacings H_1 possesses are very similar to those Blackwell observed for oriented MDI/BD hard segments.[8] This match is expected, since H_1 is an analogue of the repeating unit of the MDI/BD segment. Blackwell reported the triclinic unit cell of

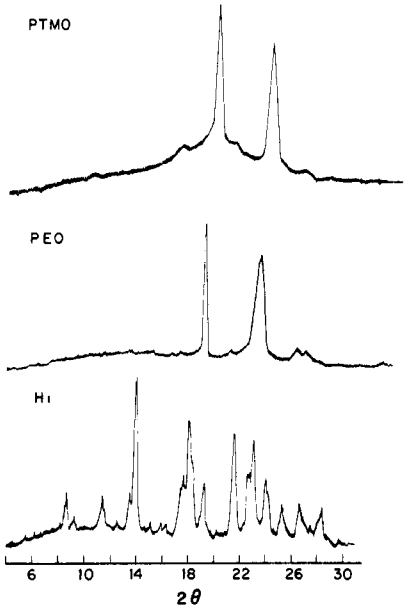

Figure 8. X-ray diffraction patterns of H_1, PEO, and PTMO at 24 °C.

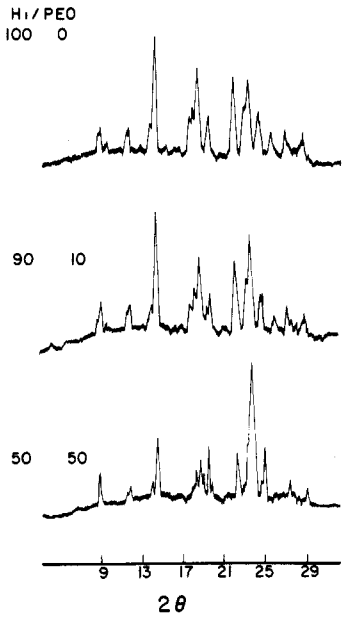

Figure 9. X-ray diffraction patterns of H_1/PEO: 100/0, 90/10, and 50/50.

MDI/BD to have the dimensions of a = 5.05 Å, b = 4.67 Å, c = 37.9 Å with α = 116°, β = 116°, and γ = 83.5°. However, in the case of H_1, the unit cell may be altered due to the presence of numerous H_1 chain ends. A higher degree of crystallinity is expected for H_1 because its low molecular weight facilitates crystallization.

Figure 9 shows the wide angle X-ray diffraction curves for H_1/PEO samples at various compositions (100/0, 90/10, and 50/50). As suggested by the phase diagram, at ambient temperature H_1/PEO (90/10) is a solid solution (β), while H_1/PEO (50/50) is a mixture of the two solid solutions, α and β, in the ratio of 7 to 10. The X-ray diffraction patterns show both H_1 and PEO diffraction peaks in the blend. It was also noticed that the addition of PEO caused no measurable change in the diffraction peak position or in the peak width of H_1. This provides a qualitative indication that the lamellar thickness of H_1 crystallites is not reduced in the H_1/PEO blends, which supports the assumption upon which the calculation of the interaction parameter for H_1/PEO pairs is based. Figure

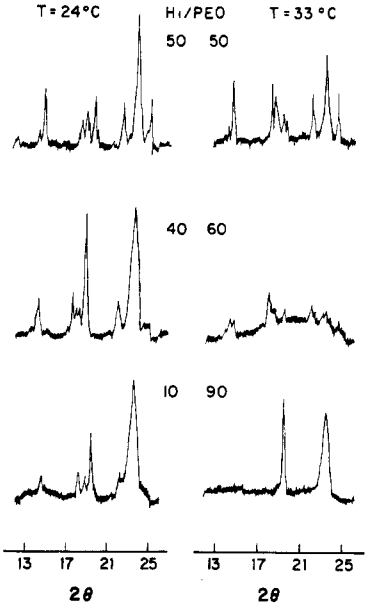

Figure 10. X-ray diffraction patterns of H_1/PEO samples at 24 and 33 °C.

10 shows the X-ray diffraction patterns of samples H_1/PEO (50/50, 40/60, and 10/90) at 24 and 33 °C which are below and above the eutectic point (31 °C). Each sample was conditioned at the desired temperature for 30 min before scanning. At 24 °C, both H_1 and PEO diffraction peaks were observed in all three compositions. This agrees with the phase diagram derived from thermal analysis, Figure 1, which suggests that these samples are a mixture of two crystalline phases, α and β, in which β is mainly composed of H_1 and α primarily of PEO. As the temperature was increased from 24 to 33 °C, H_1/PEO (50/50) exhibited only H_1 diffraction peaks and H_1/PEO (10/90) only PEO diffraction peaks. This is because H_1/PEO (50/50) and H_1/PEO (10/90) are on the opposite sides of the eutectic composition. At 33 °C, H_1/PEO (50/50) transforms into a mixture of liquid and β, while H_1/PEO (10/90) changes into a mixture of liquid and α. The X-ray diffraction is attributed to the solid solution (α or β) in both cases. It was also observed that H_1/PEO (40/60), which differs from the other blends by possessing only a single melting point at 31 °C, exhibits a largely suppressed H_1 diffraction pattern with no PEO diffraction characteristics at 33 °C. This indicates that H_1/PEO (40/60) is not the exact eutectic composition, although it is close to it.

Figure 11 shows the X-ray diffraction patterns of H_1/PEO (50/50) recorded at 24, 33, 43, 70, 90, and 100 °C. It can be observed that the PEO X-ray diffraction disappears at temperatures higher than 31 °C, while the H_1 X-ray diffraction slowly decreases with increasing temperature and finally vanishes at 100 °C. This is in agreement with thermal analysis. According to the phase diagram, the components of H_1/PEO (50/50) distribute between β and L phases in the ratio of 1/3, 1/4, 1/6, and 1/16 at temperatures of 33, 43, 70, and 90, respectively, and become all liquid at 100 °C, the liquidus point. It was also noticed that, among the diffraction peaks, those appearing at 2θ = 9, 14.4, 18.2, and 22.5° decreased at a slower rate with increasing temperature. This suggests that H_1 crystallites melt in a nonisotropic way.

Figure 12 shows the X-ray diffraction patterns of H_1/PTMO (50/50) and H_1/PPO (50/50). At 24 °C H_1/PTMO (50/50) is a mixture of β and liquid in the ratio of 7/10. The X-ray diffraction peaks are solely attributed to the

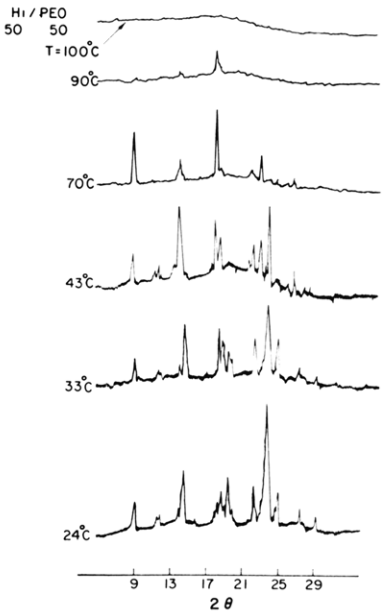

Figure 11. X-ray diffraction patterns of H_1/PEO (50/50) at 24, 33, 43, 70, 90, and 100 °C.

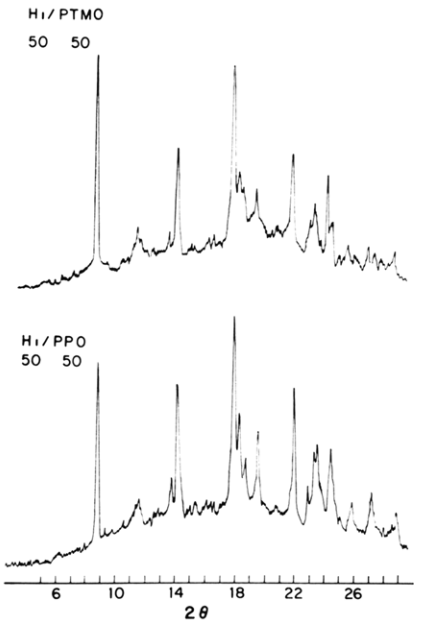

Figure 12. X-ray diffraction patterns of H_1/PPO (50/50) and H_1/PTMO (50/50) at 24 °C.

β solid solution, which is mainly composed of H_1. H_1/PPO (50/50) also has a two-phase morphology, consisting of H_1 crystals and a PPO amorphous phase. In both cases, identical H_1 diffraction patterns were observed. This again shows that the presence of polyol leads to no unusual H_1 crystalline modification.

Optical Microscopy. An optical microscope was used to study the effect of composition on the crystalline texture and the size of spherulites found in crystalline blends. Samples were cast as thin layers on glass plates and dried at 24 °C in a vacuum oven for at least 1 day. Selected samples dried for periods from 1 to 7 days all showed similar morphology.

Figure 13 shows typical optical micrographs of H_1/PEO polymer blends at the ambient temperature (24 °C). As can be observed in Figure 13a, the size of the H_1 spherulites varies from 10 to 100 μm. In the blend where H_1 and PEO are in a ratio of 9/1 and form a solid solution (Figure 13b), the spherulites all have uniform texture and are observed

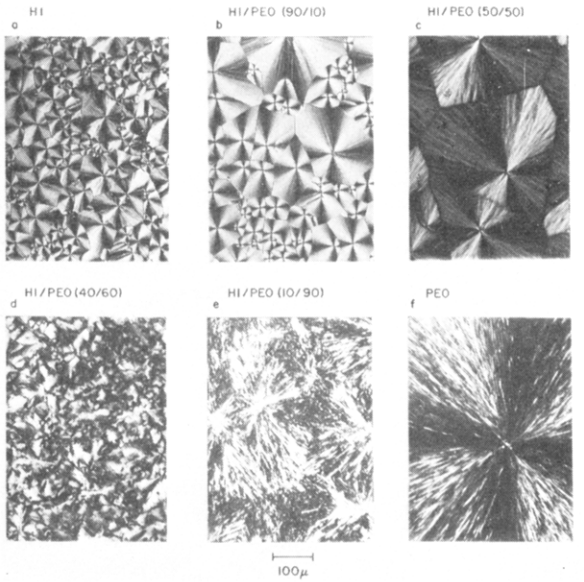

Figure 13. Optical micrographs of H_1/PEO: 100/0, 90/10, 50/50, 40/60, 10/90, and 0/100 at 24 °C.

to range in size from 30 to 100 μm, with the majority larger than 60 μm. The spherulitic structure is also more well-defined and regular than the textures observed in samples of pure H_1. Figure 13c shows a micrograph of the sample containing H_1/PEO in a 50/50 ratio, in which the H_1 and PEO are distributed in two separated crystalline phases of α and β in a ratio of 4/5. In this case an optical micrograph taken at 40 °C where the α phase has melted showed that the sizes of the spherulites are the same as that in Figure 13c. Therefore it is believed that below the eutectic melting, α and β crystal lamellae stack alternatingly in the form of radial fibrils growing from the spherulitic centers. It is important to note that there is only one spherulitic superstructure observable. Each spherulite is of the same texture and the spherulite size varies from 30 to 400 μm. Most are above 200 μm. The individual grains are in intimate contact with all adjacent grains so as to pack and fill space completely. Figure 13d is the micrograph of the sample of H_1/PEO (40/60), which contains α and β in a ratio of 4.5/3.5 and is close to the eutectic composition as suggested by both WAXD studies and thermal analysis. This composition shows no well-defined spherulites. The birefringence observed is not distributed in any symmetric or regular pattern and is probably due to the fact that one is casting close to the eutectic composition where one would normally expect finely textured crystals.

Figure 13e shows the spherulitic structure of the H_1/PEO (10/90) blend, which is a mixture of α and β phases, as suggested by X-ray diffraction. The spherulites have a different appearance than those described previously. Needle-type crystalline fibrils emanate radially from a nucleus. The bright fibrils are interspersed with dark regions, and no clearly defined grain boundaries can be observed. The spacing between two nuclei is about 200 μm. Figure 13f shows the spherulites of pure PEO. The boundaries are sharp and all the spherulites are approximately 1600 μm in diameter.

The series of optical micrographs of the H_1/PEO blends showed that the size and texture of these mostly spherulitic samples change significantly with sample composition. The spherulite sizes were smallest in pure H_1 and became larger and more well structured as the PEO was blended into H_1. The spherulite texture changed from H_1-like to PEO-like with an increasing amount of PEO, but there was

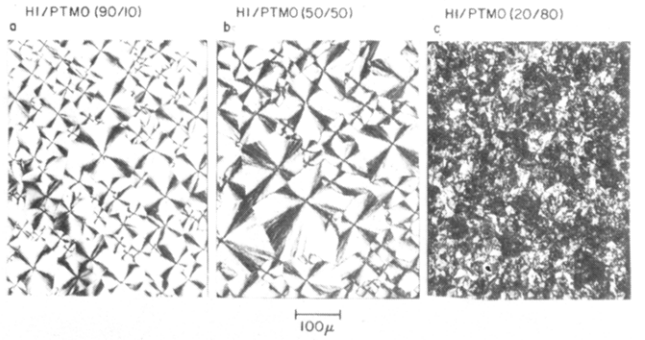

Figure 14. Optical micrographs of H_1/PTMO: (90/10), (50/50), and (20/80) at 10 °C.

basically only one type of spherulite observed at each blend composition. The increase in spherulite size indicates that the number of crystal nuclei decreases with the addition of PEO, suggesting that either nucleation is suppressed or that crystal growth is enhanced by the presence of PEO. Possibly, PEO enhances the diffusion of H_1 molecules, thereby increasing the rate of crystal growth. A comparison between pure H_1 and pure PEO shows that the spherulite size in PEO is at least 16 times larger than in H_1. This could be attributed to the fact that crystallization at room temperature (24 °C) proceeded differently for each of the H_1 and PEO phases. At 24 °C, which is far below the T_m of H_1 (129 °C), nucleation of H_1 is favored. The strong intermolecular forces such as hydrogen bonding in H_1 allow the molecules to gather and align in small parallel arrays, which serve as crystal nuclei. Subsequently, the rigidity of the H_1 molecules may hinder its diffusion, resulting in slower growth. In the case of PEO, it may take longer to create a nucleus, because the crystallization temperature was closer to the T_m of PEO (45 °C). However, in the case of PEO a higher segmental diffusion rate facilitates a higher crystal growth rate and thus larger spherulites.

Figure 14 shows the optical micrographs of three H_1/PTMO blends (90/10, 50/50, and 20/80). In order to be consistent with the microscopy carried out on the H_1/PEO system, the optical micrographs were taken below the temperature of eutectic melting at ~6 °C (T_{EU} = ~10 °C for H_1/PTMO). At this temperature, H_1/PTMO (90/10) is a solid solution while both H_1/PTMO (50/50) and (20/80) are a mixture of α and β in the approximate ratio of 4/5 and 2/7, respectively. Similar to the H_1/PEO system, the spherulites became larger and more regular as PTMO was blended with H_1. As can be observed, the spherulite sizes of H_1/PTMO (90/10) (Figure 14a) are mainly in the range between 50 and 130 μm. Spherulite sizes of H_1/PTMO (50/50) (Figure 14b) are between 100 and 200 μm. It was also found that the fibers which radiate out from the spherulitic centers are in shorter segments and the appearance of birefringence is more diffuse in the H_1/PTMO (50/50) spherulites than in H_1/PTMO (90/10) spherulites. This is due to the difference in the distribution of α vs. β phase between H_1/PTMO (50/50) and H_1/PTMO (90/10). Figure 14c shows the micrograph of H_1/PTMO (20/80), which is close to the eutectic composition. Similar to H_1/PEO (40/60), the birefringence exhibits an irregular pattern, and no spherulites are observed.

Figure 15 shows the optical micrographs of H_1/PPO (10/90) and H_1/PPO (50/50) at 24 °C. At this temperature, both H_1/PPO blends possess crystalline and amorphous phases in contrast to H_1/PEO or H_1/PTMO systems which are composed of two crystalline phases. The same features found in the blend systems of H_1/PEO and

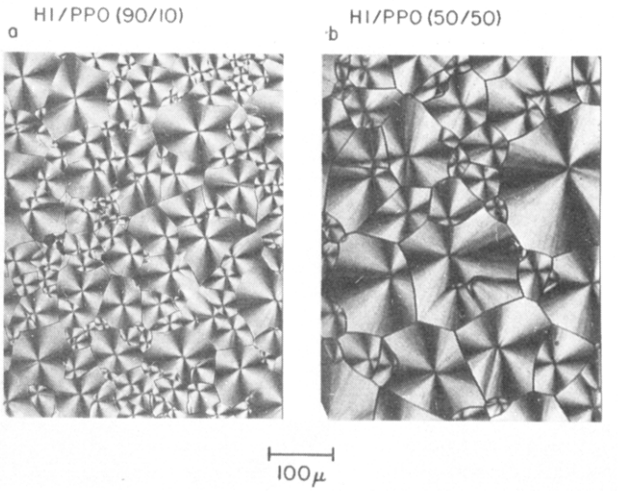

Figure 15. Optical micrographs of H_1/PPO: (90/10) and (50/50) at 24 °C.

H_1/PTMO were observed. The spherulites became larger and more well developed as the poly(propylene oxide) was blended with H_1.

It is understood that the larger the grain size of the spherulites the smaller the amount of grain boundary and the lower the grain boundary energy. Thus, the stability of the crystal is increased as polyol is blended into H_1. However, the miscibility of H_1 and the polyol also affect the melting point by lowering the blend's enthalpy in the liquid state. A careful comparison reveals that the increase in the size of spherulites by the addition of PTMO or PPO is not as substantial as the addition of PEO to H_1. This suggests that the spherulite radial growth rates are more rapid when H_1 is blended with PEO than with PTMO or PPO. In general, the spherulitic growth rate can be qualitatively described by the Lauritzen and Hoffman equation (eq 11), which originated from the modified Turnbull–Fisher equation[23,24]

$$G = G_0 \exp[-U^*/R(T - T_\infty)] \exp(-\Delta\phi^*/RT) \quad (11)$$

where G is the radial growth rate, and U^* is the activation energy for transport of crystallizable segments through the liquid to the site of the crystal. T_∞ is a hypothetical temperature where all molecular motion associated with viscous flow ceases and is related to T_g by $T_\infty = T_g - C$, where C is a constant. $\Delta\phi^*$ is the free energy required to form a critical size nucleus from the liquid and G_0 is a constant related to the initial composition. For the blends which are richer in H_1 than the eutectic composition, the presence of polyol has two significant effects on the process of crystallization. First, it lowers the activation energy, U^*, for transport of crystallizing units H_1 across the liquid–crystal interface. Second, the polyol dilutes the H_1 and weakens the interaction between H_1 molecules, causing the need for an extra amount of energy in order to gather enough H_1 molecules to form a nucleus of critical size. This explains why the size of the spherulites increases as polyols are mixed into H_1.

Conclusions

The urethane hard-segment model compound H_1, diethyl 4,4′-methylenebis(*N*-phenylcarbamate), can serve as an analogue of the repeating unit of MDI/BD hard segments in conventional polyurethane block copolymers. DSC studies reveal that blends of H_1 and PEO give rise to a eutectic composition at a weight ratio of ~40/60 (H_1/PEO) with T_{ME} = 31 °C. H_1 and PTMO also form a eutectic at about 20/80 (H_1/PTMO) with T_{ME} = 10 °C.

According to the Flory–Huggins theory, the higher the degree of polymerization of the polyol and the lower the value of the H_1–polyol interaction parameter, the higher the polyol concentration as well as T_{ME} of the eutectic composition. In contrast to the PEO and PTMO systems, poly(propylene oxide) (PPO) is intrinsically an amorphous compound and forms a crystalline–amorphous phase diagram with H_1.

Wide angle X-ray diffraction revealed that the presence of the polyol, as well as variations in temperature up to the liquidus point, did not alter the crystal form of H_1. This suggests that the melting point depression observed is a result of the excess free energy released during mixing, which allows determination of the H_1/polyol interaction parameter using Scott's equation. The interaction parameter densities of H_1/polyol pairs at their melting points were found to be $B_{H_1/PEO} = -4.63$ cal/cm^3, $B_{H_1/PTMO} = -3.41$ cal/cm^3, and $B_{H_1/PPO} = -1.21$ cal/cm^3. The negative values of B indicate H_1 and the polyols (PEO, PTMO, and PPO) form compatible liquids.

The morphology of H_1/polyol blends was studied with a polarizing microscope. Distinct spherulites were observed for pure H_1 and H_1/polyol blends. With the addition of polyols, the spherulite radii increase and the texture of the spherulites change from maltese cross patterns to radiating fibrous morphologies, especially for those blends that are of high PEO or PTMO content. The spherulites of H_1/PEO systems are larger in size than those of H_1/PTMO or H_1/PPO. This may be due to the fact that H_1 and PEO possess a strong interaction (suggested by the low value of $B_{H_1/PEO}$) which makes PEO a more effective diluent for hindering nucleation in H_1. In addition, the presence of PEO may also ease the transport of the crystallizing H_1 units across the liquid–crystal interface, resulting in larger spherulites.

Acknowledgment. We acknowledge partial support of this work by the Polymers Section of the NSF Division of Materials Research through Grant DMR 81-06888 and by the Naval Air Systems Command through Contract N00019-82-C-0246. We also thank Jen Kai Chen for carrying out part of the thermal analysis study.

Registry No. H_1, 10097-16-2; PEO, 25322-68-3; PPO, 25322-69-4; PTMO, 25190-06-1.

References and Notes

(1) S. L. Cooper and G. M. Estes, Eds., "Multiphase Polymers", American Chemical Society, Washington, DC, 1979, Adv. Chem. Ser. No. 176.
(2) R. Bonart and E. H. Muller, *J. Macromol. Sci. Phys.*, **B10**, 345 (1974).
(3) J. W. C. Van Bogart, Ph.D. Dissertation, University of Wisconsin, 1981.
(4) Y. Camberlin, and J. P. Pascault, *J. Polym. Sci., Polym. Chem. Ed.*, **21**, 415 (1983).
(5) Y. Camberlin, J. P. Pascault, M. Letoffe, and P. Caludy, *J. Polym. Sci., Polym. Chem. Ed.*, **20**, 383 (1982).
(6) J. Blackwell and K. H. Gardner, *Polymer*, **20**, 13 (1979).
(7) J. Blackwell, M. R. Nagarajan, and T. B. Hoitink, *Polymer*, **23**, 950 (1982).
(8) J. Blackwell and M. Ross, *J. Polym. Sci., Polym. Lett. Ed.*, **17**, 447 (1979).
(9) H. Tadokoro, Y. Chatani, T. Yoshihara, S. Tohara, and S. Murahashi, *Makromol. Chem.*, **73**, 109 (1964).
(10) C. P. Buckley and A. J. Kovacs, *Colloid Polym. Sci.*, **254**, 695 (1976).
(11) H. Tadokoro, Y. Takahashi, Y. Chatani, and H. Kakida, *Makromol. Chem.*, **109**, 96 (1967).
(12) H. Kakida, D. Makino, Y. Chatani, M. Kobayashi, and H. Tadokoro, *Macromolecules*, **3**, 569 (1970).
(13) R. L. Scott, *J. Chem. Phys.*, **17**, 279 (1949).
(14) T. Nishi and T. T. Wang, *Macromolecules*, **8**, 909 (1975).
(15) R. L. Imken, D. R. Paul, and J. W. Barlow, *Polym. Eng. Sci.*, **16**, 593 (1976).
(16) T. Nishi, *J. Macromol. Sci., Phys.*, **B17**, 517 (1980).
(17) W. W. Wendlandt, "Thermal Methods of Analysis", Wiley, New York, 1974.
(18) K. Nakayama, T. Ino, and I. Matsubara, *J. Macromol. Sci., Chem.*, **A3**, 1005 (1969).
(19) J. C. Wittmann and R. St. John Manley, *J. Polym. Sci., Polym. Phys. Ed.*, **15**, 2277 (1977).
(20) C. B. Wang and S. L. Cooper, *Macromolecules*, **16**, 775 (1983).
(21) L. Mandelkern, "Crystallization of Polymers", McGraw-Hill, New York, 1964.
(22) K. K. S. Hwang, G. Wu, S. B. Lin, and S. L. Cooper, *J. Polym. Sci., Polym. Chem. Ed.*, accepted for publication.
(23) T. T. Wang and T. Nishi, *Macromolecules*, **10**, 42 (1977).
(24) J. I. Lauritzen, Jr. and J. D. Hoffman, *J. Appl. Phys.*, **44**, 4340 (1973).

Miscibility of Ethylene–Vinyl Acetate Copolymers with Chlorinated Polyethylenes. 3. Simulation of the Spinodal Using the Equation of State Theory

Shamsedin Rostami and David J. Walsh*

Department of Chemical Engineering and Chemical Technology, Imperial College, London SW7, England. *Received June 20, 1983*

ABSTRACT: Chlorinated polyethylene and ethylene–vinyl acetate copolymers have previously been shown to be miscible and to phase separate on heating. In this paper a spinodal equation based on Flory's equation of state theory was derived and applied to the phase diagrams of these mixtures. Using values of the interactional parameter, X_{12}, derived from heats of mixing measurements, it was found that the predicted spinodal curves could not match the cloud point curves unless the entropy correction term containing Q_{12} was used. Also the predicted curves were flatter than the cloud points, suggesting an overestimation of X_{12}. The excess volume change on mixing was also calculated and was found to be larger than the measured value. This can also be improved by introducing Q_{12} and by using a lower value of X_{12}.

Introduction

In previous papers we have described the miscibility of various ethylene–vinyl acetate copolymers (EVA) with chlorinated polyethylenes (CPE).[1,2] This was demonstrated by the presence of single glass transition temperatures intermediate between those of the pure polymers. We also have measured the cloud point curves of the mixtures.[1] They phase separate on heating, showing a lower critical solution temperature (LCST). The LCST was higher for polymers with a higher content of vinyl

0024-9297/84/2217-0315$01.50/0